Using High Frequency Ultrasound Envelope Statistics to Determine Scatterer Number Density in Dilute Cell Solutions

A.S. Tunis[1,2], R. E. Baddour[1,2], G. J. Czarnota[2], A. Giles[2], A. E. Worthington[2], M. D. Sherar[1,2], and M. C. Kolios*[1,3]
[1]University of Toronto, Department of Medical Biophysics, Toronto, Ontario, Canada,
[2]Ontario Cancer Institute, University Health Network, Toronto, Ontario, Canada,
[3]Ryerson University, Department of Physics, Toronto, Ontario, Canada.
*email: mkolios@ryerson.ca

Abstract— **It has previously been demonstrated in tissue-mimicking phantoms and in tissue that envelope statistics of US backscatter are affected by changes in the scatterer properties [1–4, 32, 37]. At higher frequencies the wavelength of the US begins to approach the size of cells and cellular components and at this scale the envelope statistics of HFUS backscatter become more sensitive to structural changes within cells. To investigate the relation between the envelope statistics and cell structure, experiments were performed in vitro. The physical meaning of the fit parameters was evaluated by investigating HFUS backscatter from suspensions of various concentrations of two different cell lines of different sizes.**

Keywords – High-Frequency; Ultrasound; Envelope Statistics; Cell

I. INTRODUCTION

In most ultrasound imaging, the resulting image is produced from the envelope of the signal. The amplitude of the envelope has a statistical distribution that is determined by the properties of the scatterers. The statistical distribution of the envelope of ultrasound backscatter signals can thus be used to differentiate between different tissue types. A number of theoretical studies and investigations with phantoms have shown the relationship between signal statistics and scatterer properties. Groups at Drexel University (Philadelphia, PA, USA) have developed a theoretical framework relating signal envelope statistics to scatterer properties [1-4]. There have been a number of investigations into the use of signal statistics for differentiating tissue types in vivo. Shankar et al. have demonstrated the use of signal statistics for detecting tumours and differentiating between benign and malignant breast tumours [1,5,6]. Hao et al. demonstrated that a similar technique could differentiate reperfused myocardium from infarcted tissue [7]. More recently, Raju et al. demonstrated that the same techniques could be extended to higher frequencies (30MHz) to differentiate between different skin types [8].

The sensitivity of HFUS to structural changes in cells has the potential to be used for a number of applications. A prime example is monitoring the response of tumours to anti-cancer therapies. In the response of tumours to anti-cancer therapies, there is often an apoptotic response of the cells [9]. Currently during a treatment regimen, the patient must undergo a full treatment cycle before an evaluation of the treatment outcome can be made, usually by assessing the reduction in tumour size by physical examination and, less frequently, imaging. Using HFUS to quantify the structural changes occurring in cells during apoptosis and necrosis could provide a non-invasive technique to evaluate the response of tumours to therapy. This evaluation could be made much earlier in the treatment cycle, sparing the patient population from unnecessary treatment comorbidity.

II. METHODS

The data were acquired using the VisualSonics VS-40B HFUS scanner (VisualSonics Inc., Toronto, Ontario, Canada). This is a modified version of the commercial device and is able to acquire raw RF data along with B-scan images. The device was used with a 20MHz f# 2.35 transducer also manufactured by VisualSonics.

A region of interest (ROI) was selected in the B-scan image, then RF data were acquired from approximately 200 lines separated by at least one beamwidth within the ROI. The RF data were stored in tagged ultrasound file format (TUFF) along with details of the acquisition including the transducer used, the acquisition settings and a B-scan image of the ROI. Using a custom program written in JAVA (JDK 1.4.1, Sun Microsystems, Inc., Santa Clara, CA, USA), the TUFF file was reopened and the B-scan ROI displayed along with the focus of the transducer and the location of the RF lines. Within the file, a homogeneous ROI 1mm deep centered on the focus was selected. The RF data from this ROI were then extracted and the gain applied during acquisition removed.

After extraction of the RF data from the TUFF files, the rest of the analysis was done in Matlab (The MathWorks Inc., Natick, MA, USA) using the Statistics, Optimization, Symbolic and Signal toolboxes. Before the analysis the data were corrected for attenuation. Since the data were selected from a 1mm deep ROI centred on the focus, which is well within the depth of field of the transducer, any drop in signal over the depth of the ROI was due mainly to the effect of attenuation. To correct for this, the attenuation in dB/mm was determined as the decrease in mean signal envelope over the 1mm depth. Using this attenuation value the data were corrected for

attenuation by applying depth dependant amplification. The trends observed were not significantly changed when attenuation correction was not applied.

To obtain the fit parameter values of the theoretical PDFs to the acquired data, the maximum likelihood estimation (MLE) technique was implemented in Matlab. This is an iterative process using the Nelder-Mead Simplex method to optimize the fit [10].

To gain a better understanding of the physical interpretation of the statistical fit parameters, an elegant experiment was performed using dilutions of two different sized cell lines in suspension. This experiment demonstrates the relationship between the fit parameters and the number density and size of cells. The experiments were performed twice, displaying similar trends.

Separate cultures of acute myeloid leukemia cells (OCI-AML5) and prostate adenocarcinoma cells (PC-3) were grown. The AML cells were grown at a cell density of 3 x 105cells/ml in α minimum essential medium (GIBCO 11900, Rockville, MD, USA) supplemented with 5% fetal bovine serum (Cansera International, Etobicoke, ON, Canada) at 37°C. The PC-3 cells were grown in Kaighn's modification of Ham's F12 medium (GIBCO 21127, Rockville, MD, USA) supplemented with streptomycin (100mg/L) and penicillin (100mg/L) and 10% fetal bovine serum (Cansera International, Etobicoke, ON, Canada) at 37°C. As the PC-3 cells are adherent, before experiments the cells were trypsinized. A volume of each type of cells was measured, and then diluted with a corresponding volume of phosphate buffered saline (PBS) solution in a sample holder to form suspensions with various volume concentrations of cells. B-scan images and RF data from approximately 200 locations separated by at least one beamwidth were acquired from the samples of cells (Figure 1). Following the data acquisition, images of the individual cells were acquired with a light microscope to estimate the cell diameter.

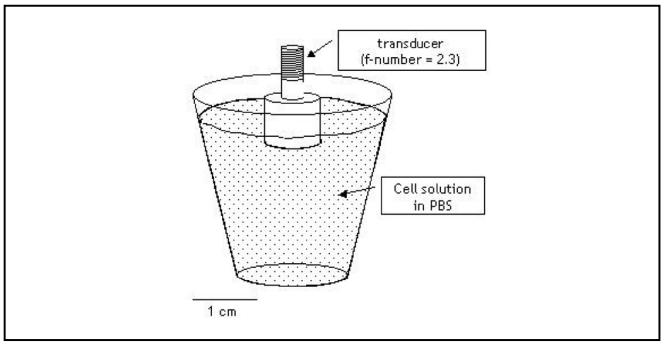

Figure 1. Schematic of setup for cell dilution experiments. A set volume of cells was placed in a plastic container filled with PBS to generate solutions with a known concentration of cells.

III. RESULTS

The light microscopy images (Figure 2) reveal the large difference in diameter of the two cell lines. Because of the larger size of the PC-3 cells, at the same volume concentration of cells, the suspension of AML cells will have 14 times more cells per volume than the corresponding suspension of PC-3 cells. This is clearly visible in the B-scan images where at the low volumetric concentrations, such as 0.025%, individual cells are visible in the image (Figure 3). As the concentration of cells increases the image formed displays a speckle pattern formed from signal contributions from a large number of cells within the resolution volume of the transducer.

As the volumetric concentration of cells in the solution is increased up to 1.6% cells by volume the mean of the signal increases. This is also reflected in the shape of the histograms of the signal amplitude for both cell lines (Figure 4). The PC-3 pellet has a higher mean signal intensity than the PC-3 1.6% solution. The AML pellet has a lower mean signal intensity than the AML 1.6% solution, likely due to the different scattering interactions for cells in solution and cells in a pellet.

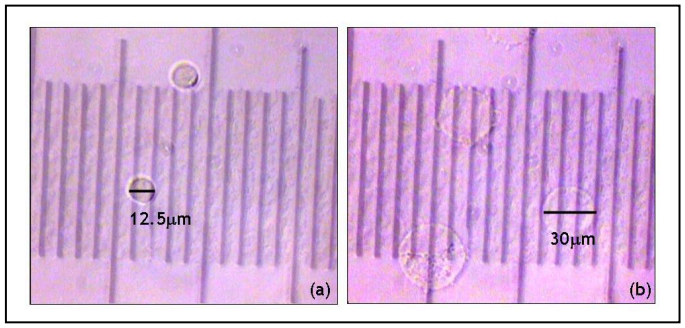

Figure 2. Phase contrast light microscopy images of AML cells (a), and PC-3 cells (b). The images are superimposed on a scale bar where every minor division is 10μm, the AML cells have an average diameter of 12.5μm while the PC-3 cells have an average diameter of 30μm.

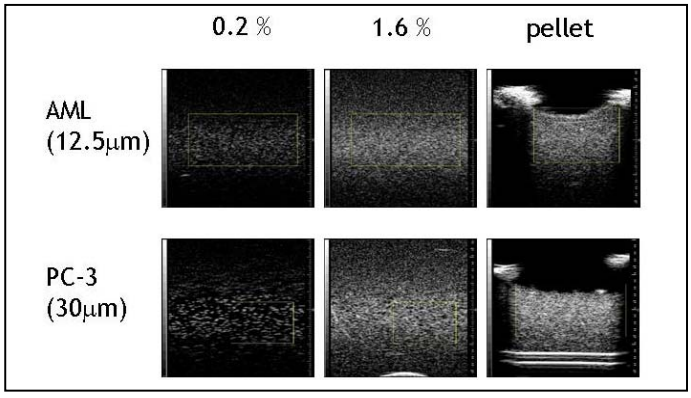

Figure 3. B-scan images (8 x 8mm) of the suspensions of various concentrations of AML cells (top row) and PC-3 cells (bottom row). At the lower concentrations individual cells are apparent, however as the concentration is increased the B-scan shows the speckle pattern characteristic of US images. While the AML pellet appears darker than the 1.6 % concentration solution, the PC-3 pellet does not, implying differences in the scattering interaction in solution vs. pellet.

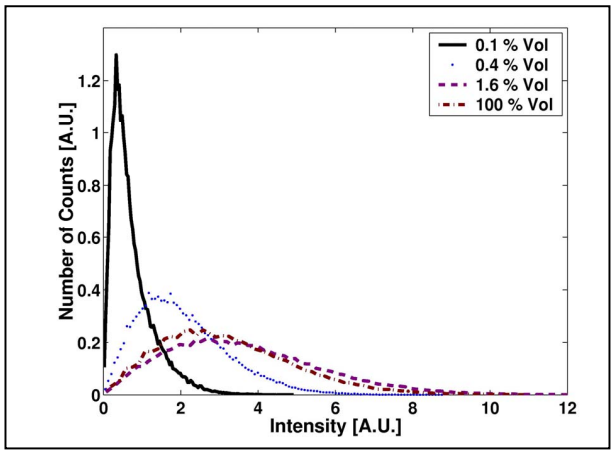

Figure 4. Histograms of signal amplitude for AML cells in suspension at various volumetric concentrations and pellets (100% cells). The histograms are normalized to an area of one. The shape of the histogram progresses to higher mean values for all concentrations in solution.

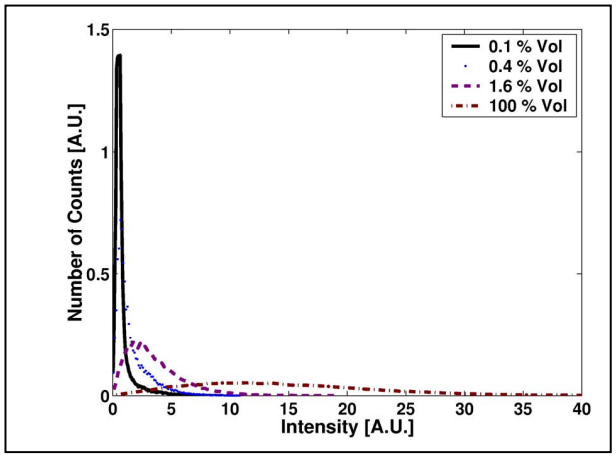

Figure 5. Histograms of signal amplitude for PC-3 cells in suspension at various volumetric concentrations and pellets (100% cells). The histograms are normalized to an area of one. The shape of the histogram progresses to higher mean values for all concentrations in solution.

The GG PDF fit parameters were determined for the data acquired from the cells in suspension and in pellets. By plotting the GG PDF fit parameters against the calculated number density instead of volumetric concentration certain trends became apparent. The number density was determined based on the concentration used and assuming cell diameters of 12.5µm and 30µm for the AML and PC-3 cells respectively. For example, a solution containing 1.6% by volume of 12.5µm cells would have $1.5x10^4$cells/mm^3. The GG a parameter, representing effective scatterer cross-section, increases with the number density of cells in suspension (Figure 6). As well, at the number densities where the AML and PC-3 overlap the GG a parameter for the PC-3 cells was larger than the GG a parameter for the AML cells. As the diameter of the PC-3 cells is more than twice that of the AML cells, it would be expected that they have a larger effective scatterer cross-section. While the trend does not continue from cells in suspension to cells in pellets for the AML cells, the PC-3 cells do have a higher a GG a parameter than the AML cells.

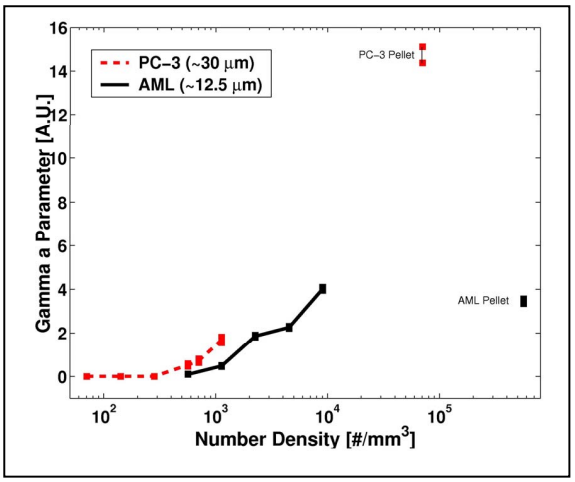

Figure 6. The GG a parameter with 95 % confidence intervals for HFUS data from suspensions of AML and PC-3 cells. The number density was determined based on the concentration used and assuming uniform cell sizes. The GG a parameter is higher at every number density for the larger PC-3 cells than the smaller AML cells. This agrees with the interpretation of GG a as the effective scatterer cross-section.

The GG c/v parameter also shows an increasing trend with increasing number density. There is a considerable overlap between the two cell lines in the range where the number densities are similar (Figure 6). The results indicate that in sparse solutions of cells the c/v parameter can provide an estimate of scatterer number density independent of the size of the scatterers being evaluated. This agrees with the predictions of Shankar [11] that the c/v parameter relates to the effective scatterer number density. Again the trend does not continue from cells in suspension to cells in pellets, however as might be expected, the AML cells do have a higher c/v parameter than the PC-3 cells.

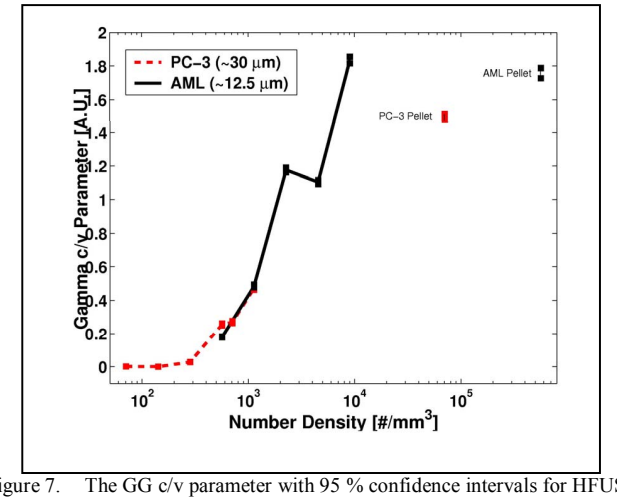

Figure 7. The GG c/v parameter with 95 % confidence intervals for HFUS data from suspensions of AML and PC-3 cells. The number density was determined based on the concentration used and assuming uniform cell sizes. The GG c/v parameter increases with number density for both cell types. This agrees with the interpretation of GG c/v as the effective scatterer number density.

IV. DISCUSSION

HFUS data were collected from dilute suspensions of AML and PC-3 cells to assess the physical interpretation of the GG fit parameters. The results demonstrate that the GG fit parameters can be related to physical properties of scatterers in a cell system. As described by Shankar [11] the a parameter depends on the effective scatterer cross-section (Figure 5), and the ratio of c/v depends on the effective scatterer number density (Figure 6). This was confirmed in the experimental results, indicating that effective scatterer cross-section and number density can be evaluated using HFUS signal statistics from sparse solutions of cells.

In the pellets of AML and PC-3 cells, similar trends are observed; the larger cells (PC-3) have a higher scale parameter, corresponding to a larger effective cross-section. The smaller cells (AML) have a higher ratio of c/v, corresponding to the higher number density of cells in a pellet. The difference in the parameters between the suspensions and pellets of the same cells indicates that there is a different scattering interaction in cells in suspension and pellets of cells. Evidence to date has indicated that in pellets the nucleus is a primary scattering source [12–14], it is believed that in suspension the major interaction would be at the cell membrane/suspension solution itself. Further evidence from the spectroscopic analysis of this data indicates that this is indeed the case [14]. While in the AML cells the nucleus is approximately 90% of the diameter of the cell, in the PC-3 cells the nucleus is smaller relative to the cell. Because of the relatively smaller size of the PC-3 nuclei, they can be located more randomly within the cell, compared to the AML nuclei which are restricted to a fairly small region. This allows for a more random distribution of the nuclei within the pellet for the PC-3 cells compared to the AML cells. It has been shown that an increased randomization leads to an increase in the GG a parameter [15]. The decreased randomization in the pellet compared to the solution may be one reason producing the large difference observed in the GG parameters between the pellets and solutions of cells (Figures 5 and 6). Thus these parameters really provide a measure of effective scatterer cross-section and number density. It may not be possible to relate them rigorously to actual scatterer cross-section and number density, as the parameters may be affected by a number of physical properties of the scatterers. The parameters are however related to physical properties of scatterers, and they can be used to monitor changes in scatterer properties in dilute solutions. More experiments, with higher concentrations of cells, are currently underway to further examine the relationship of the GG a and c/v parameters, and rigorously measure the cell sizes and concentrations.

V. CONCLUSIONS

The results of this investigation demonstrate that HFUS signal statistics are affected by physical properties of cells. Initial experiments with dilutions of AML and PC-3 cells demonstrated that the GG a and c/v parameters can be related to the effective scatterer cross-section and number density respectively. This relationship was originally demonstrated by Shankar et al. [11] in work with simulations and tissue-mimicking phantoms. These experiments demonstrated the applicability of this relationship to a biological system in vitro.

ACKNOWLEDGMENT S

The authors would like to acknowledge the generous support of the Whitaker Foundation (grants RG-01-0141) and the Natural Sciences and Engineering Research Council (NSERC, CHRP grant 237962-2000). The VisualSonics ultrasound imaging instrument was purchased with the financial support of the Canada Foundation for Innovation, the Ontario Innovation Trust and Ryerson University.

REFERENCES

[1] P. M. Shankar, J. M. Reid, H. Ortega, C. W. Piccoli, and B. B. Goldberg. Use of non-rayleigh statistics for the identification of tumors in ultrasonic b-scans of the breast. IEEE Trans Med Imaging, 12(4):687–692, 1993.

[2] P. M. Shankar. A model for ultrasonic scattering from tissues based on the k distribution. Phys Med Biol, 40(10):1633–49, 1995.

[3] P. M. Shankar et al. Studies on the use of non-rayleigh statistics for ultrasonic tissue characterization. Ultrasound Med Biol, 22(7):873–82, 1996.

[4] P. M. Shankar. A compound scattering pdf for the ultrasonic echo envelope and its relationship to k and nakagarni distributions. IEEE Trans Ultrason Ferroelectr Freq Control, 50(3):339–343, 2003.

[5] P. M. Shankar et al. Classification of ultrasonic b-mode images of breast masses using nakagami distribution. IEEE Trans Ultrason Ferroelectr Freq Control, 48(2):569–80, 2001.

[6] P. M. Shankar et al. Classification of breast masses in ultrasonic b scans using nakagami and k distributions. Phys Med Biol, 48(14):2229–40, 2003.

[7] X. Hao, C. J. Bruce, C. Pislaru, and J. F. Greenleaf. Segmenting high-frequency intracardiac ultrasound images of myocardium into infarcted, ischemic, and normal regions. IEEE Trans Med Imaging, 20(12):1373–83, 2001.

[8] B. I. Raju and M. A. Srinivasan. Statistics of envelope of high-frequency ultrasonic backscatter from human skin in vivo. IEEE Trans Ultrason Ferroelectr Freq Control, 49(7):871–82, 2002.

[9] M. A. Barry, C. A. Behnke, and A. Eastman. Activation of programmed cell death (apoptosis) by cisplatin, other anticancer drugs, toxins and hyperthermia. Biochem Pharmacol, 40(10):2353–62, 1990.

[10] William H. Press, Saul A. Teukolsky, William T. Vetterling, and Brian P. Flannery. Numerical Recipes in FORTRAN: The art of scientific computing, 2nd ed. Cambridge University Press, New York, 2 ed, 1992.

[11] P. M. Shankar. Ultrasonic tissue characterization using a generalized nakagami model. IEEE Trans Ultrason Ferroelectr Freq Control, 48(6):1716–1720, 2001.

[12] J. Beaulieu et al. High-frequency ultrasound characterization of microcellular components. In Proceedings of the 10th Congress of the World Federation for Ultrasound in Medicine and Biology, page S123, Montreal, Canada, 2002.

[13] G. J. Czarnota. Ultrasound imaging of apoptosis in vivo: Effects of subcellular nuclear morphology and cell membrane morphology. In Proceedings of the 10th Congress of the World Federation for Ultrasound in Medicine and Biology, page S117, Montreal, Canada, 2002.

[14] M. C. Kolios, G. J. Czarnota, A. E. Worthington, A. Giles, A. S. Tunis, and M. D. Sherar. Towards understanding the nature of high frequency backscatter from cells and tissues: An investigation of backscatter power spectra from different concentrations of cells of different sizes. In IEEE Ultrasonics Symposium, Montreal, Canada, 2004.

[15] A.S. Tunis, G.J. Czarnota, A. Giles, M.D. Sherar, J.W. Hunt and M.C. Kolios. Monitoring structural changes in cells with high-frequency ultrasound signal statistics. Ultrasound Med Biol, 31(8):1041-1049, 2005.